Spectrochimica Acta Part A: Molecular and Biomolecular Spectroscopy 129 (2014) 173–183

Contents lists available at ScienceDirect

Spectrochimica Acta Part A: Molecular and Biomolecular Spectroscopy

journal homepage: www.elsevier.com/locate/saa

On the origins of the absorption spectroscopy of pterin and $Re(CO)_3(pterin)(H_2O)$ aqueous solutions. A combined theoretical and experimental study

Ezequiel Wolcan *

Instituto de Investigaciones Fisicoquímicas Teóricas y Aplicadas (INIFTA, UNLP, CCT La Plata-CONICET), Diag. 113 y 64, (B1906ZAA) La Plata, Argentina

HIGHLIGHTS

- TD-DFT study of the absorption spectroscopy of pterin and $Re(CO)_3(pterin)(H_2O)$ complex as a function of pH.
- NBO and DOS analyses.
- $\pi \rightarrow \pi^*$, $n \rightarrow \pi^*$ and $n \rightarrow n$ transitions responsible for the lowest energy band of pterin.
- MLLCT transitions responsible for the lowest energy band of Re(I) complex.

GRAPHICAL ABSTRACT

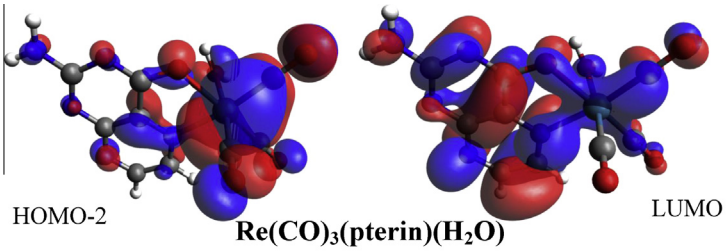

HOMO-2 is composed of 48% of Re, 24% of CO and 27% of pterin character. LUMO is composed of more than 91% of pterin character. The lowest energy band of $Re(CO)_3(pterin)(H_2O)$, HOMO-2→LUMO, is a MLLCT transition.

ARTICLE INFO

Article history:
Received 19 December 2013
Received in revised form 10 March 2014
Accepted 16 March 2014
Available online 24 March 2014

Keywords:
Pterin
Re(I)-tricarbonyl complex
UV–vis spectroscopy
Acid–base
TD-DFT
MLLCT

ABSTRACT

The origins of the absorption spectroscopy of pterin and $Re(CO)_3(pterin)(H_2O)$ complex as a function of pH is studied using the hybrid functional B3LYP and PBE0 in combination with 6-311++G(d,p) and LanL2TZ(f) basis sets. A natural bond analysis was performed to the principal molecular orbitals involved in the electronic transitions of the studied compounds. The low energy band of pterin, which is described as a H → L electronic transition, can be interpreted as an admixture of $\pi \rightarrow \pi^*$, $n \rightarrow \pi^*$ and $n \rightarrow n$ electronic transitions involving π(C2–N1, C6–N5, C9–C10) and n(C2) orbitals of the HOMO and π^*(C6–N5, C7–N8) and n(C4) orbitals of the LUMO. The low energy band of $Re(CO)_3(pterin)(H_2O)$ can be described as a combination of different MLLCT transitions where electron density residing on different π orbitals of carbonyl-Re bonds and lone pairs of Re is transferred to pterin moiety. Besides MLLCT transitions, IL, LLCT and LLMCT transitions contribute the absorptions of the Re(I) complex in the wavelength region corresponding to the high energy bands. The calculated electronic spectra of the acid and base forms of pterin and $Re(CO)_3(pterin)(H_2O)$ were simulated from the theoretical results and compared to the experimental absorption spectra with great accuracy both in position and relative intensities of the absorption bands.

Introduction

Rhenium (I) carbonyl–diimine complexes of the type *fac*-ReX$(CO)_3$(α-diimine) are thermally and photochemically robust and highly flexible synthetically. The photophysics and photochemistry of the Re(I) chromophore is affected by structural variations in the α-diimine ligands as well as the axial ligand X. Therefore, a rational design in the synthesis of the α-diimine ligands was used to tune the photophysical and photochemical properties of the metal complexes in order to obtain photosensitizers that might be utilized in broad research areas such as electron

* Tel.: +54 2214257430.
E-mail address: ewolcan@inifta.unlp.edu.ar

http://dx.doi.org/10.1016/j.saa.2014.03.022
1386-1425/

transfer studies [1], solar energy conversion [2–4], catalysis [5], luminescent sensors [6–8], molecular materials for non-linear optics [9,10] and optical switching [11]. In particular, luminescent transition metal complexes of Re(I) and Ru(II) with polypyridil ligands have been recognized as good candidates for the development of pH sensing devices [12–14].

As these complexes show exceptionally rich excited-state behavior and redox chemistry as well as thermal and photochemical stability [15,16], they have also been used as biological labeling reagents and non-covalent probes for biomolecules and ions [17–19]. In this regard, some complexes including biologically relevant ligands like substituted pterins coordinating the $-Re(CO)_3Cl$ core have been synthesized and characterized [20–22]. Pterins (2-amino-4-oxo(3H)-pteridine, Scheme 1a) are heterocyclic compounds amply distributed in nature. Substituted pterins derivatives at the 6 position are usually found in biological systems such as pigments, one-carbon transfer cofactors and redox cofactors. Such biological significance has attracted considerable interest in the study of their properties and reactivity *in vitro* and also *in vivo* [23,24].

In previous work, we have synthesized and characterized a new water soluble complex, $Re(CO)_3(pterin)(H_2O)$ (see Scheme 1b). Protonation studies in aqueous solutions of the Re(I) complex showed two acid–base equilibriums with $pK_{a1} = 3.9$ and $pK_{a2} = 8.8$. pK_{a1} was assigned to the protonation equilibrium at N1 of pterin ligand in the complex and pK_{a2} could be ascribed to the deprotonation of coordinated water molecule [25]. In this paper, we re-examine the UV–vis absorption spectroscopy of pterin and $Re(CO)_3(pterin)(H_2O)$ by time-dependent density functional theory (TD-DFT) calculations in combination with Natural Bonding Orbital (NBO) and density of state (DOS) analyses. The nature of the electronic absorption spectra of pterin (PT) and $Re(CO)_3(PT)(H_2O)$ acid–base forms is discussed. The low energy band of pterin, which is responsible for its observed luminescence [24], can be described as a $(\pi_{C2-N1}, \pi_{C6-N5}, \pi_{C9-C10}, n_{N2}) \rightarrow (\pi^*_{C6-N5}, \pi^*_{C7-N8}, n_{C4})$ transition, i.e. an admixture between $\pi \rightarrow \pi^*$, $n \rightarrow \pi^*$ and $n \rightarrow n$ transitions. On the other hand, the low energy band of $Re(CO)_3(PT)(H_2O)$ can be described as a combination of different metal–ligand-to-ligand charge transfer (MLLCT) transitions where electron density residing on different π orbitals of carbonyl-Re bonds and lone pairs of Re is transferred to PT moiety. Besides MLLCT transitions, intra-ligand, ligand-to-ligand charge transfer (LLCT) and ligand-to-ligand–metal charge transfer (LLMCT) transitions contribute the absorptions of the Re(I) complex in the wavelength region corresponding to the high energy bands.

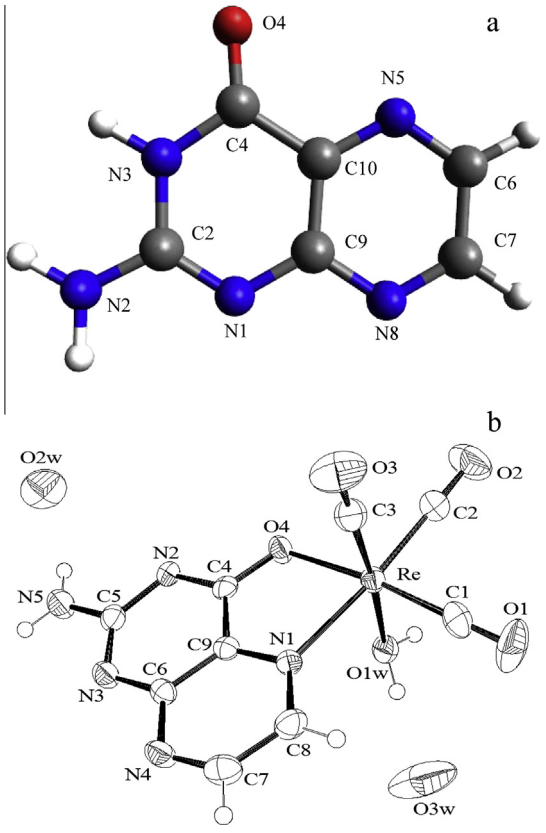

Scheme 1. (a) 2-Amino-4-oxo(3H)-pteridine, pterin (PT). (b) Ortep view of $Re(CO)_3(PT)(H_2O)\cdot 2H_2O$ molecule showing the labeling of the non-H atoms and their displacement ellipsoids at the 50% probability level. O2w and O3w are the oxygens from the two crystallization water molecules. Note that the crystallographic numbering (Scheme b) differs from the numbering according to the heterocyclic nomenclature (Scheme a). The Ortep view of $Re(CO)_3(PT)(H_2O)\cdot 2H_2O$ was drawn from the CIF file of Ref. [25].

Computational details

DFT and TD-DFT calculations of ground and excited state properties of a series of Re(I) tricarbonyl complexes have been recently employed to interpret the experimental absorption bands arisen from a set of MLCT, LLCT and IL transitions [26–35]. The electronic structures of pterin and Re(I) tricarbonyl complex were determined using tools of DFT [36–38] as implemented in Gaussian 09 package [39]. The optimization of the ground state geometry was carried out by means of the three-parameter hybrid functional developed by Becke [40] in conjunction with the LYP [41] exchange potential (B3LYP) with the LanL2DZ basis set which uses Dunning D95V basis set on C, N, O, H [42] and Los Alamos ECP plus DZ on Re [43–45]. Vibrational frequencies were computed at the same level of theory to confirm that these structures were minima on the energy surfaces. These calculations were checked for accuracy by comparison to X-ray crystallographic data obtained for Re(I) tricarbonyl complex. The experimental values of a number of bond distances and angles are shown in Table 1. They are in good agreement with those obtained by DFT, with bond lengths differing in less than 0.1 Å and bond angles by 3° or less. The vertical transition energies were calculated at the optimized ground-state geometry by TD-DFT [46–48] using the following set of hybrid functionals: B3LYP, CAM-B3LYP, X3LYP and PBE0. The general performance of the these hybrid functionals, as evidenced by the best match between calculated and experimental electronic transitions, was B3LYP > PBE0 for pterin while PBE0 > B3LYP ≈ X3LYP > CAM-B3LYP for the Re(I) complex. Therefore, all the electronic transitions presented hereafter are those calculated using B3LYP functional for pterin and PBE0 for the Re(I) complex. In all TD-DFT calculations, 6-311++G(d,p) basis set was used for C, N, O and H atoms while LanL2TZ(f) [49,50] (triple zeta basis set designed for an ECP plus f polarization) was used for Re atom. Both optimized geometries and TD-DFT calculations were carried out including solvent effects (water) through the Polarizable Continuum Model [51–53] to produce a number of 110 singlet-to-singlet transitions. A natural bond analysis (NBO) was performed to the principal molecular orbitals (MOs) involved in the electronic transitions of the studied compounds in order to ascertain the contributions of the different molecular fragments to the UV–vis spectroscopy using the NBO program (version 3.1) implemented within Gaussian 09 [54]. Percentage compositions of different molecular fragments to MOs and DOS spectra from output files generated from Gaussian 09 were calculated using the AOMix program [55,56]. Absorption spectra were simulated with Gaussian distributions with a full-width at half-maximum (fwhm) set to 3000 cm^{-1} with the aid of GaussSum 2.2.5 program.

Table 1
Experimental and DFT-calculated bond lengths (Å) and angles (°) around rhenium ion in $Re(CO)_3(PT)(H_2O)$.

	Crystal structure[a]	B3LYP/LanL2DZ
Bond lengths (Å)		
Re–C(3)	1.889(5)	1.900
Re–C(1)	1.896(6)	1.909
Re–C(2)	1.920(5)	1.924
Re–O(4)	2.162(3)	2.160
Re–N(1)	2.185(3)	2.188
Re–O(1W)	2.190(3)	2.204
C(4)–O(4)	1.283(5)	1.326
C(4)–N(2)	1.326(6)	1.339
C(5)–N(2)	1.368(5)	1.390
C(5)–N(5)	1.327(6)	1.360
Angles (°)		
C(3)–Re–C(1)	89.1(2)	90.1
C(3)–Re–C(2)	88.8(2)	90.5
C(1)–Re–C(2)	89.1(2)	90.8
C(3)–Re–O(4)	95.04(17)	96.9
C(1)–Re–O(4)	173.66(17)	171.1
C(2)–Re–O(4)	95.85(17)	94.6
C(3)–Re–N(1)	92.90(17)	92.9
C(1)–Re–N(1)	98.37(17)	97.4
C(2)–Re–N(1)	172.39(17)	171.1
O(4)–Re–N(1)	76.62(12)	76.9
C(3)–Re–O(1W)	174.55(16)	173.6
C(1)–Re–O(1W)	94.71(18)	95.2
C(2)–Re–O(1W)	95.15(17)	93.0
O(4)–Re–O(1W)	80.88(12)	77.5
N(1)–Re–O(1W)	82.67(12)	82.9

[a] Taken from Ref. [25]. The numbering of C, N and O atoms corresponds to the crystallographic numbering of Scheme 1b.

Results and discussion

UV–vis spectroscopy of pterin aqueous solutions

In aqueous solutions, pterin, 2-amino-4-oxo-3*H*-pteridine, behaves as a weak acid and the amide group is in equilibrium with the phenolate group, Eq. (1), with a p*K*a of ca. 8 [24].

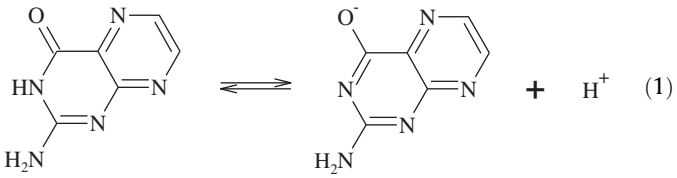

(1)

The absorption spectrum of pterin at pH = 6, where acid form (PT) is prevalent, shows three main absorption bands centered at 340, 270 and 230 nm corresponding to electronic transitions from ground singlet state (S_0) to excited states S_1, S_2 and S_3, respectively. The basic form of pterin, PTO^-, which is dominant at pH > 8, shows only two absorption bands centered at 252 and 358 nm. The calculated TD-DFT results are summarized and compared with experimental data in Table 2 for PT and PTO^-. It is observed that the main spectral features are predicted to a great accuracy, both in position and relative intensities, by TD-DFT calculations. The main MOs involved in the most intense electronic transitions are the highest occupied molecular orbital (HOMO), the lowest unoccupied molecular orbital (LUMO), H−5, H−3, and L+1 for PT and HOMO, LUMO H−5, H−2, and L+1 for PTO^-. Fig. 1. shows spatial plots of those MOs for PT and PTO^-. It is observed that they are very similar in shape. However, MOs for PTO^- are shifted by about 0.6–0.8 eV to higher energies than those of PT.

The calculation of an electronic structure of a given electronic state yields its corresponding molecular energy and wave function (ψ). Since ψ is dependent on the coordinates of all the electrons, it is not very suitable for interpretation. Thus, simplified notions and characteristics of ψ are required to get a deeper insight into the electronic structure of molecules. Mulliken population analysis (MPA) is the most widely used procedure to get information on electronic structure of molecules. The AOMIX program takes advantage of MPA to calculate, for instance, density-of-states (DOS). Plots of DOS spectra provide a pictorial representation of MO compositions based on the contributions of the different fragments in which the whole molecule can be split for analysis. The DOS spectra were generated from contributions of nine molecular fragments: O, N2, N3, C4, C6–N5, C7–N8, C2–N1, C9–C10 and all the H atoms (See Scheme 1a for atom numbering). The DOS plot generated with AOMIX from these nine fragments for PT is shown in Fig. 2. A simple inspection to the DOS plot at the energy corresponding to a particular MO will give, after comparison with the total density of states (TDOS), the percentage contribution of each fragment to that particular MO. For instance, Fig. 2. shows that the HOMO of PT (MO energy = −6.72 eV at the B3LYP/6-311++G(d,p) level of theory) is composed mainly by the orbitals of C2–N1 (around 30%) with a lesser contribution of the orbitals of C9–C10, C6–N5 and N2 (about 15–20% each) and even lesser contributions of O4 and C7–N8. C4, N3 and H fragments do not contribute to that MO. This proportional description of HOMO is fully consistent with its plot shown in Fig. 1. On the other hand, the LUMO (energy = −2.47 eV) is mostly composed of orbitals from the C7–N8 (about 35%) and C6–N5 (around 25%) fragments, with lesser contributions from C9–C10 (10%), C4 (10%) and O4 (7.5%). C2–N1, N3, N2 and H fragments do not contribute to LUMO. Therefore, the electronic transition observed at 340 nm, which is predicted by TD-DFT at 333.58 nm as a H → L transition, can be interpreted from the fragments DOS plot. This transition represents, mainly, electronic density charge transferred from the orbitals of C2–N1 and N2 fragments to the orbitals of C7–N8 and C4 fragments. In the same way, the other electronic transitions can be interpreted from the DOS plot. Thus, the electronic transition observed at 270 nm, which is predicted by TD-DFT at 260.72 nm as a H → L+1 transition, represents, mainly, electronic density charge transferred from the orbitals of N2, O4 and C2–N1 to the orbitals of C9–C10, C6–N5 and N3 fragments. The electronic transition observed at 230 nm, which is predicted as a H−3 → L transition at 230.76 nm is

Table 2
Comparison of experimental absorption data with TD-DFT calculations for PT and PTO^-.

Compound	λ_{obs}/nm ($\varepsilon/10^3$ M^{-1} cm^{-1})	λ_{calc}/nm (f_{osc})	Electronic transitions (% coefficients)
Pt	215(15.0)	214.89 (0.2948)	H−5 → L (84%)
	230 (12.4)	230.76 (0.1331)	H−3 → L (93%)
	270 (11.8)	263.44 (0.2866)	H → L+1 (89%), H−3 → L (5%)
	340 (5.6)	333.58 (0.126)	H → L (97%)
PtO^-	219(8.4)	217.62 (0.1895)	H−5 → L (86%)
		228.72 (0.0731)	H−2 → L+1 (94%)
	252 (19.5)	260.72 (0.3745)	H → L+1 (79%), H−2 → L (14%)
	358(6.6)	355.02 (0.1329)	H → L (97%)

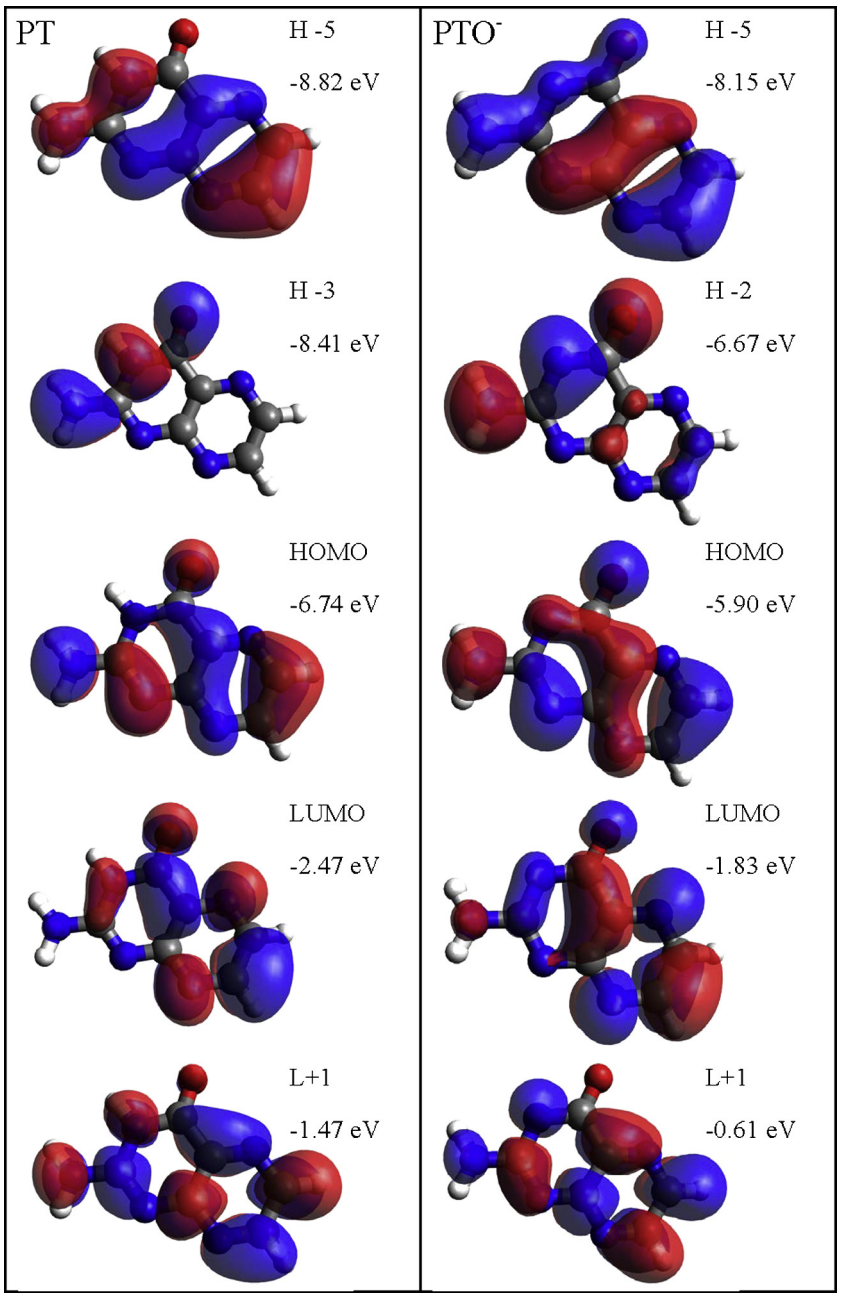

Fig. 1. Main molecular orbital diagrams (isovalue = 0.02) for PT and PTO^-. HOMO and LUMO are the major MOs involved in the low energy band for both PT (λ_{max} = 340 nm) and PTO^- (λ_{max} = 358 nm). In the wavelengths region corresponding to the high energy bands (200–280 nm), H−5 → L, H−3 → L and H → L+1 transitions account for the absorption spectrum of PT while H−5 → L, H−2 → L+1 and H → L+1 transitions describe the absorption spectrum of PTO^-. Optimized geometries and TD-DFT calculations were carried out including solvent effects (water) through the Polarizable Continuum Model.

accounted by an electronic density charge transferred from the orbitals of N3, N2 and O4 fragments to the orbitals of C6–N5, C7–N8, C9–C10 and C4 fragments. The higher energy electronic transition observed for PT at 215 nm and predicted to be a H−5 → L transition at 214.89 nm is represented mainly by an electronic density charge transferred from the orbitals of C2–N1, C7–N8 and C9–C10 fragments to the orbitals of C6–N5 fragment. The calculated electronic spectra of PT and PTO^- are simulated from the theoretical results to ease the comparison with experimental data. They are compared with their calculated spectra obtained by summing Gaussian functions centered at each calculated wavelength with the maxima related to the value of the oscillator strengths (which are also plotted) using Eq. (2)

$$\varepsilon(\tilde{\upsilon}) = \frac{2.175 \times 10^8\ \mathrm{Lmol^{-1}cm^{-2}}}{\Delta_{1/2}\tilde{\upsilon}}(f_{osc})\exp\left[-2.772\left(\frac{\tilde{\upsilon}-\tilde{\upsilon}_{i\to f}}{\Delta_{1/2}\tilde{\upsilon}}\right)^2\right] \quad (2)$$

This is the formula that GaussSum uses to convolute spectra [57]. In this equation, the parametrical value of the fwhm of the band is given in units of cm^{-1} and is symbolized by $\Delta_{1/2}\tilde{\upsilon}$, f_{osc} is the oscillator strength and $\tilde{\upsilon}_{i\to f}$ is the frequency (in units of cm^{-1}) corresponding to the wavelength of the calculated electronic transition. The simulations are shown in Fig. 3. in comparison with the experimental absorptions. The comparison is quite satisfactory and the simulated spectra follow the observed absorptions with great accuracy both in position and relative intensities.

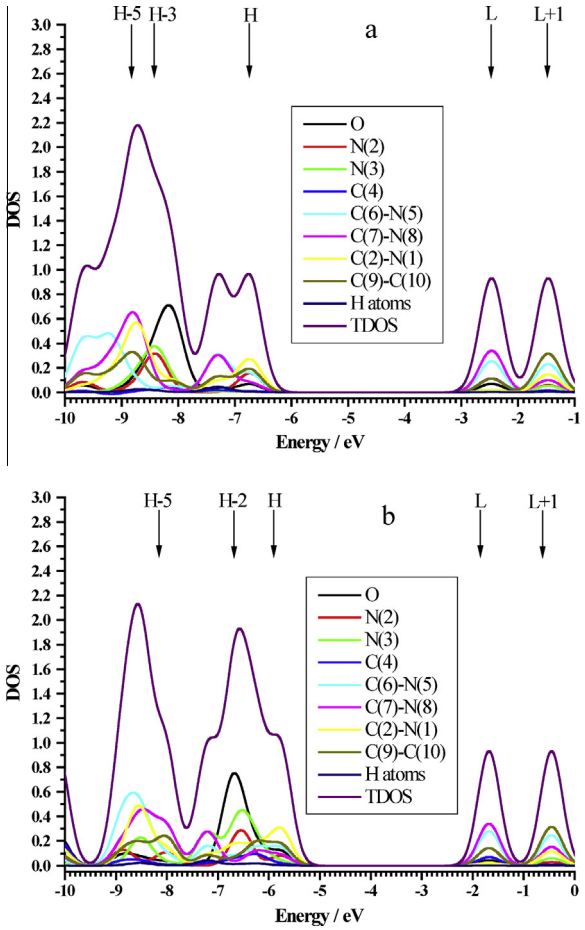

Fig. 2. Total density of states (TDOS) and partial density of states (DOS) plots generated from contributions of nine molecular fragments (O, N2, N3, C4, C6–N5, C7–N8, C2–N1, C9–C10 and all the H) for (a) PT and (b) PTO^-. The arrows mark the position in energy of the different MOs. In this plot the numbering of C, N, O atoms corresponds to the heterocyclic nomenclature numbering of Scheme 1a. See text for details.

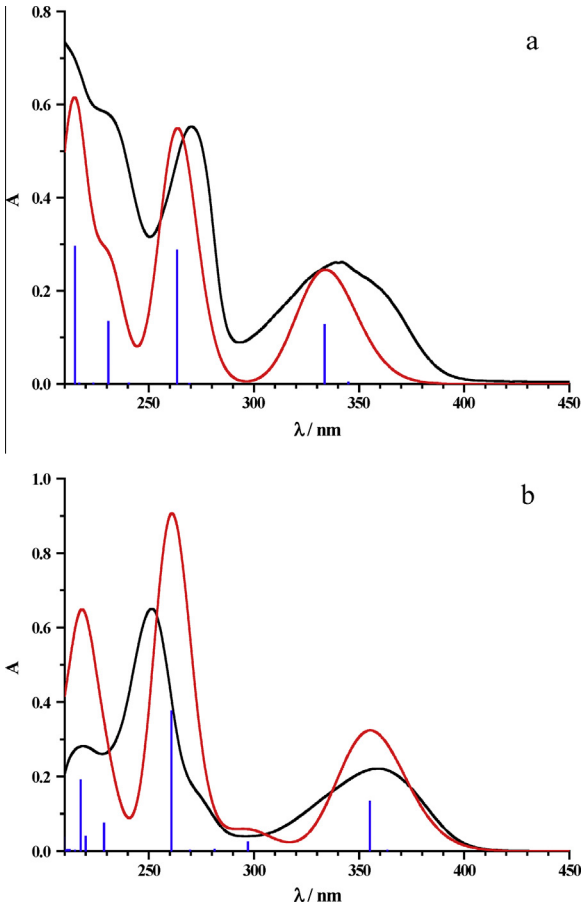

Fig. 3. Comparison of the UV–vis absorption spectrum (black lines) with TD-DFT calculated electronic transitions (blue lines) and simulated spectra (red lines) for (a) PT and (b) PTO^-. See text for details. (For interpretation of the references to color in this figure legend, the reader is referred to the web version of this article.)

A NBO analysis was performed over MOs to get a better understanding on the nature of the electronic transitions involved in the spectroscopy of the compounds. NBO analysis is based on a method for optimally transforming a given wave function into localized form, corresponding to the one-center (lone pair) and two-center (bonds) elements of the chemist's Lewis structure picture. In NBO analysis, the input atomic orbital basis set is transformed via natural atomic orbitals (NAOs) and natural hybrid orbitals (NHOs) into natural bond orbitals (NBOs). The NBOs obtained in this fashion correspond to the widely used Lewis picture, in which two-center bonds and lone pairs are localized. All these natural localized sets are complete and orthonormal, able to exactly describe any property of ψ [58]. Briefly, NBO analysis yields a description of all the MOs as a linear combination of each NBO:

$$\Psi = \sum_{i}^{N} c_i (\mathrm{NBO})_i \tag{3}$$

The index i runs over the N number of AOs which comprise the basis set chosen to describe the particular MO (i.e. N = total number of AOs = total number of MOs). Each NBO_i is described in terms of a superposition of two NHOs corresponding to two neighboring bonded atoms. For a localized σ-bond between atoms A and B, the NBO is:

$$\sigma_{AB} = c_A h_A + c_B h_B \tag{4}$$

where h_A and h_B are the NHOs centered on atoms A and B. NBOs closely correspond to the picture of localized bonds and lone pairs as basic units of molecular structure, so that is possible to conveniently interpret calculated wave-functions in terms of the classical Lewis structure concepts by transforming these functions to NBO form [58]. These localized NBO may be of different four kinds: BD for 2-center bond, CR for 1-center core pair, LP for 1-center valence lone pair, RY for 1-center Rydberg, and BD^* for 2-center anti-bond. Since DOS and spatial MOs plots for PT and PTO^- are very similar, NBO analysis was only performed on PT. The application of NBO analysis to MOs of PT yielded the following expressions in terms of leading (>5%) NBO contributions to MOs of PT relevant to the electronic transitions, Eqs. (5)–(9)

$$\psi_{H-5} \approx 0.6109\pi_{C7-N8} - 0.4702\pi_{C9-C10} - 0.317\pi_{C2-N1} + 0.2958n_{N3} + 0.2885\pi^*_{C6-N5} + 0.2384\pi^*_{C2-N1} \tag{5}$$

$$\psi_{H-3} \approx 0.6167n_{N3} - 0.5879n_{N2} - 0.5106n_{O4} \tag{6}$$

$$\psi_{H} \approx 0.3151\pi_{C6-N5} - 0.4234\pi_{C9-C10} + 0.5246\pi_{C2-N1} - 0.4143n_{N2} + 0.2751n_{O4} + 0.2762\pi^*_{C7-N8} + 0.2517\pi^*_{C6-N5} \tag{7}$$

$$\psi_{L} \approx 0.2286\pi_{C6-N5} - 0.2345\pi_{C9-C10} - 0.3327n_{C4} + 0.2763n_{O4} - 0.5952\pi^*_{C7-N8} - 0.4761\pi^*_{C6-N5} \tag{8}$$

Table 3
Comparison of experimental absorption data with TD-DFT calculations for $Re(CO)_3(PT)(H_2O)$, $[Re(CO)_3(PT)(OH)]^-$ and $[Re(CO)_3(PTH)(H_2O)]^+$.

Compound	λ_{obs}/nm (ε/ $10^3 M^{-1}cm^{-1}$)	λ_{calc}/nm (f_{osc})	Electronic Transitions (% coefficients)
$Re(CO)_3(PT)(H_2O)$		231.60 (0.1538)	H−7 → L (72%), H−3 → L+4 (4%), H−2 → L+2 (3%), H → L+2 (3%), H → L+3 (2%)
		245.99 (0.0606)	H−2 → L+2 (33%), H−2 → L+3 (20%), H−7 → L (4%), H−4 → L+2 (4%), H−3 → L+2 (7%), H−3 → L+3 (3%), H−2 → L+1 (9%), H−1 → L+2 (4%), H−1 → L+3 (7%), H → L+3 (3%)
		246.54 (0.0889)	H−1 → L+2 (16%), H−1 → L+3 (36%), H → L+3 (21%), H−7 → L (5%), H−2 → L+1 (2%), H−2 → L+2 (7%), H−1 → L+1 (3%)
	255 (16.8)	257.59 (0.1848)	H−5 → L (11%), H → L+1 (18%), H → L+2 (19%), H−7 → L (4%), H−3 → L+2 (7%), H−3 → L+3 (8%), H−2 → L+4 (3%), H−1 → L+1 (3%), H−1 → L+2 (3%), H−1 → L+3 (5%), H−1 → L+4 (2%), H → L+3 (6%)
		258.98 (0.0799)	H−3 → L+2 (20%), H−3 → L+3 (28%), H−2 → L+4 (11%), H−5 → L (6%), H−2 → L+1 (5%), H−2 → L+3 (3%), H → L+1 (4%), H → L+2 (8%), H → L+3 (5%)
	367 (6.8)	367.93 (0.1406)	H−3 → L (34%), H−2 → L (44%), H−1 → L (19%)
		371.69 (0.1004)	H−1 → L (59%), H → L (24%), H−3 → L (5%), H−2 → L (8%)
$[Re(CO)_3(PT)(OH)]^-$		222.32 (0.0511)	H−1 → L+4 (26%), H−1 → L+6 (40%), H−5 → L+1 (7%), H−1 → L+15 (2%), H → L+8 (7%), H → L+10 (2%)
		226.25 (0.0714)	H−10 → L (10%), H−3 → L+4 (19%), H−9 → L (6%), H−3 → L+2 (3%), H−3 → L+15 (3%), H−2 → L+3 (2%), H−1 → L+6 (9%), H−1 → L+9 (5%), H−1 → L+11 (4%), H−1 → L+15 (3%), H → L+5 (5%), H → L+8 (3%)
		228.63 (0.0798)	H−10 → L (44%), H−9 → L (26%), H−3 → L+4 (9%), H−1 → L+4 (3%)
		242.62 (0.0532)	H−2 → L+2 (22%), H → L+4 (18%), H → L+6 (12%), H−10 → L (3%), H−3 → L+2 (3%), H−3 → L+4 (3%), H−1 → L+3 (3%), H−1 → L+4 (5%), H−1 → L+6 (3%), H → L+5 (4%), H → L+7 (2%), H → L+10 (2%), H → L+12 (3%)
		252.38 (0.0985)	H−2 → L+1 (15%), H → L+5 (17%), H → L+8 (23%), H → L+9 (14%), H−6 → L (4%), H → L+10 (2%), H → L+11 (5%), H → L+13 (3%)
	255 (18.4)	253.21 (0.2453)	H−6 → L (11%), H−2 → L+1 (49%), H−5 → L (3%), H−1 → L+4 (2%), H → L+5 (7%), H → L+8 (9%), H → L+9 (4%)
	373 (6.5)	371.81 (0.0958)	H−2 → L (90%), H−3 → L (4%)
		417.18 (0.1413)	H−1 → L (96%)
$[Re(CO)_3(PTH)(H_2O)^+$		226.41 (0.0676)	H−8 → L (63%), H−7 → L (10%), H−2 → L+4 (4%), H−1 → L+4 (4%), H → L+4 (6%)
		227.46 (0.1211)	H−7 → L (14%), H−3 → L+3 (70%), H → L+3 (8%)
		228.63 (0.2116)	H−7 → L (48%), H−8 → L (8%), H−6 → L (2%), H−3 → L+1 (4%), H−3 → L+3 (8%), H−2 → L+4 (5%), H−2 → L+5 (4%), H → L+4 (8%), H → L+5 (2%)
	242 (14.2)	235.73 (0.0763)	H−6 → L (83%), H−7 → L (3%), H−3 → L+2 (8%)
		260.57 (0.0983)	H−3 → L+1 (62%), H → L+3 (11%), H−7 → L (4%), H−2 → L+2 (4%), H−1 → L+2 (4%), H → L+2 (3%)
	274 (7.1)	262.87 (0.1012)	H−3 → L+1 (18%), H−2 → L+1 (17%), H−2 → L+2 (12%), H → L+3 (17%), H−7 → L (4%), H−1 → L+1 (5%), H−1 → L+2 (5%), H−1 → L+5 (2%), H → L+2 (4%)
	345 (5.5)	369.79 (0.0654)	H−3 → L (94%), H → L (3%)
		406.82 (0.1119)	H−2 → L (41%), H−1 → L (27%), H → L (28%), H−3 → L (3%)

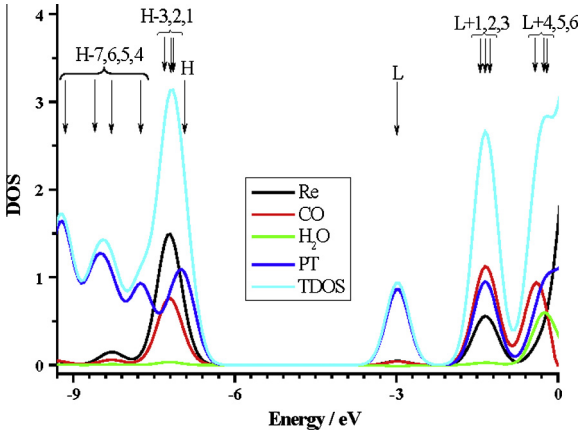

Fig. 4. Total density of states (TDOS) and partial density of states (DOS) plots for $Re(CO)_3(PT)(H_2O)$ generated from contributions of four fragments: Re atom, the three carbonyls, water molecule and PT. The arrows mark the position in energy of the different MOs. See text for details.

Table 4
Composition (% character) of relevant molecular orbitals of $Re(CO)_3(PT)(H_2O)$ as extracted from DOS and TDOS analysis of Fig. 4.

MO (energy/eV)	% Re	% CO	%H_2O	% Pt
H−7 (−9.14)	2.0	2.0	<0.1	96.0
H−6 (−8.6)	4.3	1.9	0.2	93.7
H−5 (−8.29)	11.0	5.0	<0.1	83.0
H−4 (−7.74)	11.1	5.6	0.2	83.1
H−3 (−7.29)	50.0	25.0	<0.1	24.0
H−2 (−7.20)	48.0	24.0	<0.1	27.0
H−1 (−7.14)	46.0	23.0	<0.1	30.0
H (−6.92)	33.0	17.0	<0.1	50.0
L (−2.98)	4.0	4.0	<0.1	92.0
L+1 (−1.43)	21.0	42.0	<0.1	36.0
L+2 (−1.35)	21.0	42.0	<0.1	36.0
L+3 (−1.25)	21.0	43.0	<0.1	35.0
L+4 (−0.42)	10.3	41.4	19.3	29.0
L+5 (−0.27)	16.1	28.7	21.2	34.0
L+6 (−0.20)	22.0	21.1	20.7	36.2

$$\psi_{L+1} \approx -0.3136\pi_{C7-N8} - 0.259\pi_{C2-N1} + 0.2337n_{N3} + 0.2343n_{N2} + 0.4399\pi^*_{C6-N5} + 0.5564\pi^*_{C9-C10} - 0.3041\pi^*_{C2-N1} \quad (9)$$

where π denote BD orbitals composed by superposition of p_z orbitals of bonded atoms and n stands for a LP. Thus, all the electronic transitions can be re-interpreted in terms of the expansions of ψ_{H-5}, ψ_{H-3}, ψ_H, ψ_L and ψ_{L+1} as linear combinations of the NBOs. Hence, the H → L transition can be viewed as a (π_{C2-N1}, π_{C6-N5}, π_{C9-C10}, n_{N2}) → (π^*_{C6-N5}, π^*_{C7-N8}, n_{C4}). H → L+1 is a (π_{C2-N1}, π_{C6-N5}, π_{C9-C10}, n_{N2}, n_{O4}) → (π_{C7-N8}, π^*_{C2-N1}, π^*_{C6-N5}, n_{N3}, π^*_{C9-C10}). H−3 → L is a "pure" n → π, π*, i.e. (n_{N3}, n_{N2}, n_{O4}) → (π_{C6-N5}, π_{C9-C10}, n_{C4}, π^*_{C6-N5}, π^*_{C7-N8}). H−5 → L is mainly a (π_{C7-N8}, π_{C9-C10}, π_{C2-N1}, π^*_{C2-N1}) → (π_{C6-N5}, n_{C4}, n_{O4}, π^*_{C7-N8}, π^*_{C6-N5}) transition.

Origins of the absorption spectroscopy of fac-XRe(CO)$_3$L complexes

The lowest absorption bands of *fac*-XRe(CO)$_3$L complexes occur in the near-UV region. Several electronic transitions are possible in the near UV-spectroscopy of those complexes such as ligand-field (LF), metal-to-ligand charge transfer (MLCT), ligand-to-ligand charge transfer (LLCT), and intra-ligand (IL) transitions. In most of the cases, charge transfer (CT) bands appear at somewhat longer

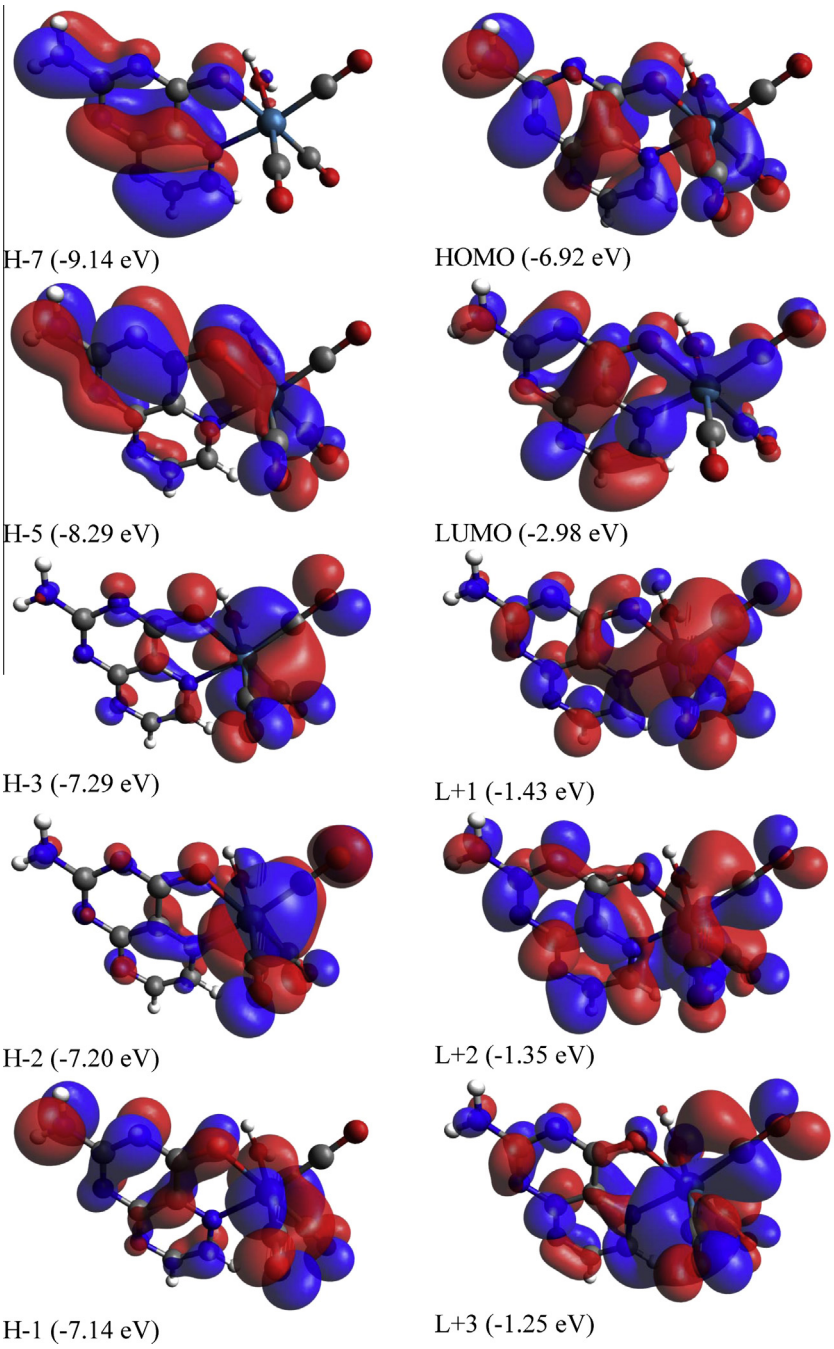

Fig. 5. Main molecular orbital diagrams (isovalue = 0.02) for Re(CO)$_3$(PT)(H$_2$O). H−1 → L, H−2 → L and H−3 → L are the main transitions involved in the low energy absorption band (λ_{max} = 367 nm) of the complex. The high energy band of the complex, λ_{max} = 255 nm, is described by H−5 → L, H → L+1 and H → L+2 transitions while H−7 → L, H−2 → L+2 and H−1 → L+3 excitations are responsible for the spectrum in the 200–240 nm wavelength region. Optimized geometries and TD-DFT calculations were carried out including solvent effects (water) through the Polarizable Continuum Model.

wavelengths (i.e. λ_{max} ~330–400 nm; $\varepsilon \sim (2\text{–}5) \times 10^3\ M^{-1}\ cm^{-1}$) than the more intense IL band, which usually peaks at $\lambda_{max} \sim$ 240–320 nm with $\varepsilon \sim 2 \times 10^4\ M^{-1}\ cm^{-1}$ [15]. Recent TD-DFT studies have questioned the appropriateness of these simplified models. Therefore, as usually mixing between MLCT/LLCT or MLCT/XLCT occur, those transitions are now generally called metal–ligand-to-ligand charge transfer (MLLCT) transitions. For instance, in complexes like $[Re(bpy)(CO)_3Cl]$ and $[Re(bpy)(CO)_3(py)]^+$ (bpy = 2,2′bipyridine, py = pyridine), the HOMO can be described as containing more than 50% of Re character, with contributions of around 20% each from CO and Cl in the case of $[Re(bpy)(CO)_3Cl]$ and 20% from CO in $[Re(bpy)(CO)_3(py)]^+$. However, the LUMO is composed of more than 80% of bpy character in both cases [16]. Therefore, the lowest energy optical transition can be assigned as having MLLCT character. Moreover, our recent TD-DFT calculations on a related water soluble Re(I) complex, $Bu_4N[(4,4'\text{-bipyridine})Re(CO)_3(dcbpy)]$ (where Bu = butyl; dcbpy = 2,2′-bipyridine-5,5′-dicarboxylate) have also shown that its lowest energy absorption band can be described as having MLLCT character [59]. LLCT excited states usually occur in complexes bearing both reducing and oxidizing type of ligands as a result of a charge transfer from one donor ligand to an acceptor ligand. There are several examples of Re(I)-tricarbonyl complexes which are known to have the lowest excited states featuring a LLCT character[16]. The extinction coefficients for such LLCT bands are usually very low due to the very weak electronic interaction between donor–acceptor in those complexes. Therefore, contrary to MLCT transitions, LLCT transitions are not usually observed directly from absorbance UV–vis spectroscopy. As in general LLCT states are non-emissive, their excited-state characteristics can be studied only by transient spectroscopy [16]. Due to the last observations, LLCT states are usually elusive when compared to MLCT states.

UV–vis spectroscopy of $Re(CO)_3(PT)(H_2O)$ aqueous solutions

The absorption spectrum of $Re(CO)_3(PT)(H_2O)$ in alkaline media, i.e. at pH = 11, consists of one intense ($\varepsilon \sim 2 \times 10^4\ M^{-1}\ cm^{-1}$) absorption centered at λ_{max} = 255 nm and an absorption band of medium intensity ($\varepsilon \sim 6 \times 10^3\ M^{-1}\ cm^{-1}$) centered at 373 nm. In neutral solutions (pH = 7) the high energy band remains virtually unaffected while the low energy band shifts to λ_{max} = 366 nm. In acidic media (pH = 2) the band at λ_{max} = 255 nm has disappeared and only a tail remains in the 220–300 nm region while in the 300–500 nm region two bands can be observed: the first one, λ_{max} = 344 nm, and the second one appearing as a broad shoulder, centered at $\lambda_{max} \sim$ 360–370 nm. Those pH dependent spectral changes, which are reversible, are due to the following protonation/deprotonation equilibriums [25]:

$$[Re(CO)_3(PTH)(H_2O)]^+ \overset{OH^-}{\underset{H^+}{\rightleftarrows}} Re(CO)_3(PT)(H_2O) \overset{OH^-}{\underset{H^+}{\rightleftarrows}} [Re(CO)_3(PT)(OH)]^-$$

where the first acid–base equilibrium involves protonation/deprotonation of N1 of coordinated pterin while the second acid–base equilibrium involves deprotonation of coordinated water molecule with pK_{a1} = 3.9 and pK_{a2} = 8.8, respectively [25].

The calculated TD-DFT results are summarized and compared with experimental data in Table 3 for $[Re(CO)_3(PTH)(H_2O)]^+$, $Re(CO)_3(PT)(H_2O)$ and $[Re(CO)_3(PT)(OH)]^-$. The main MOs involved in the most intense electronic transitions of $Re(CO)_3(PT)(H_2O)$ are H−7, H−5, H−3, H−2, H−1, HOMO, LUMO, L+1, L+2 and L+3. Fig. 4 shows DOS spectra for $Re(CO)_3(PT)(H_2O)$. The DOS spectra were generated from contributions of four fragments: Re atom, the three carbonyls, water molecule and PT. DOS spectra analysis shows that H−1, H−2 and H−3 are MOs mainly composed by contributions from Re orbitals with some contributions from COs and PT. On the other hand, H−7 and H−5 are mainly of PT character. Regarding virtual MOs, L is almost exclusively composed from PT orbitals. However, MOs L+1, L+2 and L+3 are composed of CO, PT and Re orbitals. It is noteworthy that CO ligands have higher relevance than PT ligand in L+1, L+2 and L+3 compositions. Moreover, from DOS and TDOS (Fig. 4) the contribution from each fragment to the TDOS can be calculated. The contribution (in%) from the orbitals of each fragment to the MOs of $Re(CO)_3(PT)(H_2O)$ which are relevant to the TD-DFT calculated electronic transitions are listed in Table 4. For instance (see Table 4) H−3 can be described as

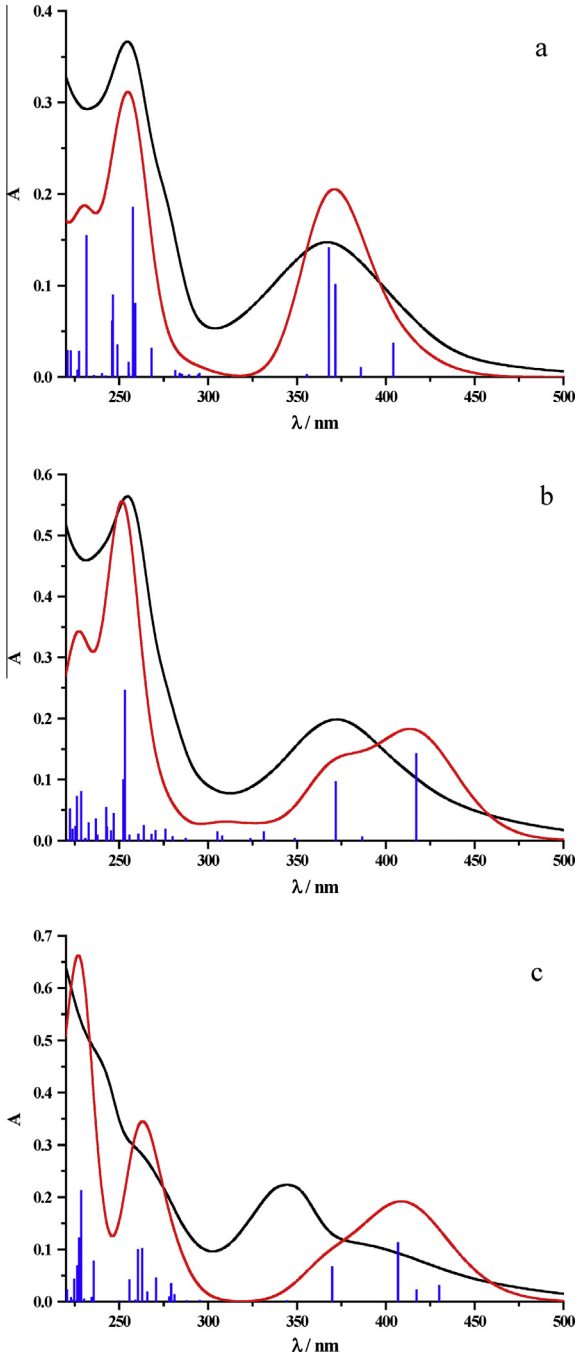

Fig. 6. Comparison of the UV–vis absorption spectrum (black lines) with TD-DFT calculated electronic transitions (blue lines) and simulated spectra (red lines) for (a) $Re(CO)_3(PT)(H_2O)$, (b) $[Re(CO)_3(PT)(OH)]^-$ and (c) $[Re(CO)_3(PTH)(H_2O)]^+$. (For interpretation of the references to color in this figure legend, the reader is referred to the web version of this article.)

containing 50% of Re character, with contributions of around 25% of CO and 24% of PT. H−2 can be described as containing 48% of Re character, with contributions of around 24% of CO and 27% of PT. Finally, H−1 can be described as containing 46% of Re character, with contributions of around 23% of CO and 30% of PT. On the other hand, L is composed of more than 91% of PT character, with only marginal (<5% each) contributions of Re and CO orbitals. TD-DFT predicts that the lower energy band of $Re(CO)_3(PT)(H_2O)$, at around 367 nm and predicted at 367.93 nm, is MLCT in nature with most of the electron density transferred from the Re–C bonds to the PT core. Since H−2 and H−3 consist mainly of π orbitals of Re–C bonds (see NBO analysis below), this is not a pure MLCT transition and should be viewed better as a $MLLCT_{Re(CO)3 \rightarrow PT}$ transition (i.e. a delocalized $Re(CO)_3 \rightarrow$ PT CT transition). Therefore, the low energy band of $Re(CO)_3(PT)(H_2O)$, which is composed of H−3 → L, H−2 → L and H−1 → L transitions, has definitely a MLLCT character. For characterization of the electronic transitions as partial CT transitions, the following definition of the CT character can be used [60]:

$$CT_I(\%) = 100(P_g(M) - P_I(M)) \quad (10)$$

where P_g(M) and P_I(M) are electronic densities on the metal in the electronic ground state and the *I*-th excited state, respectively. Positive CT_I(M) values correspond to MLCT transitions, negative CT_I(M) values correspond to LMCT transitions [60].

We can rewrite this definition by using the atomic orbital contribution to a particular MO. Therefore, the CT character for a H−n → L+m excitation is:

$$CT(\%) = \%(Re)_{H-n} - \%(Re)_{L+m} \quad (11)$$

If the excited state is formed by more than one one-electron excitation, then the metal CT character of this excited state is expressed as a sum of CT characters of each participating excitation, $i \rightarrow j$ [60]:

$$CT_I(\%) = \sum_i [C_I(i \rightarrow j)]^2 \left[\%(M)_i - \%(M)_j\right] \quad (12)$$

where $C_I(i \rightarrow j)$ are the appropriate coefficients of the *I*-th transition giving the percentage contribution of a configuration to the resulting excited state TD-DFT wavefunction. With the aid of Tables 3 and 4 and Eqs. (10)–(12), a 43% of CT character can be calculated for the low energy band of $Re(CO)_3(PT)(H_2O)$.

The high energy band of $Re(CO)_3(PT)(H_2O)$, observed at 255 nm and predicted to be at 257.59 nm, consists mainly of intra-ligand electronic transitions of PT (transition H−5 → L) and an admixture of LLMCT, LLCT and MLLCT transitions (see NBO analysis below) from PT and Re–C bonds to CO ligands (H → L+1 and L+2 transitions). Electronic transitions predicted at 231.60, 245.99 and 246.54 nm, which account for the UV part of the spectrum of the complex at $\lambda < 255$ nm, are mainly an admixture of intra-ligand electronic transitions of PT (transition H−7 → L) and MLLCT (H−2 → L+2 and H−1 → L+3) transitions. Fig. 5 shows the spatial plots for the relevant MOs involved in the electronic transitions of $Re(CO)_3(PT)(H_2O)$. These plots confirm the nature of the electronic transitions inferred from DOS analysis. Fig. 6 shows the simulated absorption spectra for $Re(CO)_3(PT)(H_2O)$, $[Re(CO)_3(PT)(OH)]^-$ and $[Re(CO)_3(PTH)(H_2O)]^+$ compared with the experimental absorptions. The comparison is quite satisfactory for $Re(CO)_3(PT)(H_2O)$ and $[Re(CO)_3(PT)(OH)]^-$ and the simulated spectra follow the observed absorptions with great accuracy both in position and relative intensities. Nevertheless, the predicted absorption spectrum for $[Re(CO)_3(PTH)(H_2O)]^+$ is somewhat less accurate. NBO analysis on $Re(CO)_3(PT)(H_2O)$ allows a precise description of the relevant MOs to the electronic transitions (again in terms of leading, i.e. >5%, NBO contributions to ψs (see Table 5)). Note the discrepancy between the numbering according to heterocyclic nomenclature and the crystallographic numbering used in Table 5 and in the following analysis. The low energy band of $Re(CO)_3(PT)(H_2O)$, Table 3, is composed of H−3 → L, H−2 → L and H−1 → L transitions. H−3 → L can be described as a combination of at least three different MLLCT transitions involving two different π orbitals of C1–Re bonds and *n* (LP) of Re plus a LLCT transition involving π orbitals of C2–O2 with the charge being transferred

Table 5
NBO analysis showing the leading contributions ($c_i^2 > 0.05$) of each NBO to relevant MOs of $Re(CO)_3(PT)(H_2O)$. Each coefficient (c_i) in this table corresponds to the coefficients that multiply each NBO_i which appear in the MO expansions as linear combinations of the NBOs (Eq. (3)).

Character	NBO_i	$c_i(\psi_{H-7})$	$c_i(\psi_{H-5})$	$c_i(\psi_{H-3})$	$c_i(\psi_{H-2})$	$c_i(\psi_{H-1})$	$c_i(\psi_H)$	$c_i(\psi_L)$	$c_i(\psi_{L+1})$	$c_i(\psi_{L+2})$	$c_i(\psi_{L+3})$	$c_i(\psi_{L+4})$
Re orbitals (LP)	n_{1Re}			−0.3843	0.6010							
	n_{2Re}								0.2525		−0.2383	
C1–Re orbitals	π_{1C1-Re}		0.2844	−0.3390	−0.3275	−0.4716	0.2182					
	π_{2C1-Re}		−0.2276	−0.5203	−0.2883	0.4157						
	$\pi^*_{1\ C1-Re}$								−0.3166			
	$\pi^*_{2\ C1-Re}$										−0.2937	0.3620
N1–Re orbitals	π^*_{N1-Re}										−0.2615	
O4–Re orbitals	π^*_{O4-Re}								−0.3183			
CO orbitals	$\pi^*_{1\ C2-O2}$			−0.2435						0.2846	0.4571	0.2291
	$\pi^*_{1\ C3-O3}$				−0.2366					0.2263	0.2632	
	$\pi^*_{2\ C2-O2}$				−0.2623				0.3653	0.2180		−0.5102
	$\pi^*_{2\ C3-O3}$								−0.3425		0.3110	0.4703
PT orbitals (LP)	n_{C6}									−0.2366		
	n_{C9}	−0.3619					−0.3503	−0.3071				
	n_{N5}	−0.3887	0.3462			0.3821	0.3740					
	n_{O1}								−0.2274			0.2449
	n_{O4}		0.3916			0.2390	−0.3024					
PT orbitals (π, π*)	π_{C4-N2}		0.6081									
	π_{C5-N3}	−0.4639										
	π_{C6-N3}		−0.2440				0.3639					
	π_{C7-N4}	0.5127								0.2310		
	π_{C8-N1}						0.2595					
	$\pi*_{C4-N2}$					−0.2170		−0.3433				
	$\pi*_{C6-N3}$						−0.3536		0.2181	−0.3945	0.2502	
	$\pi*_{C7-N4}$						0.2302	−0.5416	−0.2238			
	$\pi*_{C8-N1}$	0.2982					0.2510	−0.5269		−0.3306	0.2586	

to π^*_{C7-N4}, π^*_{C8-N1}, π^*_{C4-N2} and n_{C9} orbitals of PT. Similarly, H−2 → L is a combination of at least three different MLLCT transitions involving two different π orbitals of C1–Re bonds and *n*(LP) of Re plus two LLCT transitions involving π orbitals of C2–O2 and C3–O3 with the charge being transferred to π^*_{C7-N4}, π^*_{C8-N1}, π^*_{C4-N2} and n_{C9} orbitals of PT. Finally, H−1 → L transition can be described as two MLLCT (from two different π orbitals of C1–Re bonds to PT moiety) plus (n_{N5}, n_{O4}, π^*_{C4-N2}) → (π^*_{C7-N4}, π^*_{C8-N1}, π^*_{C4-N2}, n_{C9}) intra-ligand transitions. It is noteworthy that among the three carbonyls, only equatorial C1 participates in MLLCT transitions while C2 and C3 participate in LLCT and LLMCT transitions. The high energy band of $Re(CO)_3(PT)(H_2O)$, can be described mainly as a combination of H−5 → L, H → L+1 and H → L+2 transitions. H−5 → L is a combination of intra-ligand transitions on the PT moiety, (π_{C4-N2}, π_{C6-N3}, n_{O4}, n_{N5}) → (π^*_{C7-N4}, π^*_{C8-N1}, π^*_{C4-N2}, n_{C9}), plus two MLCCT, (π_{1C1-Re}, π_{2C1-Re}) → (π^*_{C7-N4}, π^*_{C8-N1}, π^*_{C4-N2}, n_{C9}). H → L+1 and H → L+2 are mainly combinations of MLLCT transitions plus LLCT and LLMCT transitions from PT moiety to carbonyls (C2–O2, C3–O3), O4–Re and C1–Re plus intra ligand transitions of PT. Concerning the highest energy transitions, H−7 → L is a (π_{C6-N3}, n_{N5}) → (π^*_{C8-N1}, π^*_{C4-N2}) intra-ligand electronic transition while H−2 → L+2 is composed of one MLCT and two MLLCT transitions, i.e. (n_{1Re}, π_{1C1-Re}, π_{2C1-Re}) → (π^*_{C6-N3}, π^*_{C8-N1}, $\pi^*_{1\ C2-O2}$, n_{C5}, π_{C7-N4}), from Re and C1–Re to PT moiety. On the other hand, H−1 → L+3 is composed of two MLLCT transitions from C1–Re to PT moiety plus (n_{N5}, n_{O4}, π^*_{C4-N2}) → ($\pi^*_{1\ C2-O2}$, $\pi^*_{2\ C3-O3}$, $\pi^*_{2\ C1-Re}$, $\pi^*_{1\ C3-O3}$, π^*_{N1-Re}, π^*_{C8-N1}, π^*_{C6-N3}, n_{2Re}) transitions.

Conclusions

NBO and DOS analyses in combination with TD-DFT calculations is a powerful tool which can accurately discern the nature of electronic transitions in organic molecules as well as in organometallic complexes. We have successfully applied this technique to unravel the nature of electronic absorption spectra of acid–base forms of pterin and $Re(CO)_3(PT)(H_2O)$. For the acid form of pterin, the lowest energy band, which is centered at 340 nm, corresponds to a H → L transition which can be viewed as a (π_{C2-N1}, π_{C6-N5}, π_{C9-C10}, n_{N2}) → (π^*_{C6-N5}, π^*_{C7-N8}, n_{C4}), i.e. an admixture between $\pi \rightarrow \pi^*$, $n \rightarrow \pi^*$ and $n \rightarrow n$ transitions. The calculated electronic spectra of PT and PTO^- were simulated from the theoretical results with great accuracy both in position and relative intensities of the absorption bands. On the other hand, the low energy band of $Re(CO)_3(PT)(H_2O)$ can be described as a combination of at least three different MLCT and MLLCT transitions involving two different π orbitals of C1–Re bonds and *n* of Re with the charge being transferred to PT moiety. However, the high energy bands of the Re(I) complex were identified as being combinations of MLLCT, intra-ligand transitions of PT, besides LLCT and LLMCT transitions from PT moiety to carbonyls (C2–O2, C3–O3) and C1–Re. LLCT and LLMCT transitions, which are usually difficult to observe, are clearly discerned through NBO/DOS analysis.

Acknowledgements

This work was supported in part by grants X533 (UNLP), PIP 0389 (CONICET) and PICT 2010-1435 (ANPCyT). E.W. is a research member of CONICET.

References

[1] M.A. Fox, M. Chanon, Photoinduced Electron Transfer, Elsevier, Amsterdam, 1988.
[2] V. Balzani, F. Bolletta, M. Gandolfi, M. Maestri, Bimolecular electron transfer reactions of the excited states of transition metal complexes, in: Org. Chem. Theory, Springer, Berlin / Heidelberg, 1978, pp. 1–64.
[3] M. Grätzel, Energy Resources Through Photochemistry and Catalysis, Academic Press, New York, 1983.
[4] K. Kalyanasundaram, Photophysics, photochemistry and solar energy conversion with tris(bipyridyl)ruthenium(II) and its analogues, Coord. Chem. Rev. 46 (1982) 159–244.
[5] K. Kalyanasundaram, M. Grätzel, Photosensitization and Photocatalysis Using Inorganic and Organometallic Compounds, Kluwer Academic Publishers, Dordrecht, 1993.
[6] L. Sacksteder, M. Lee, J.N. Demas, B.A. DeGraff, Long-lived, highly luminescent rhenium(I) complexes as molecular probes: intra- and intermolecular excited-state interactions, J. Am. Chem. Soc. 115 (1993) 8230–8238.
[7] V.W.-W. Yam, K.M.-C. Wong, V.W.-M. Lee, K.K.-W. Lo, K.-K. Cheung, Synthesis, photophysics, ion-binding studies, and structural characterization of organometallic rhenium(I) crown complexes, Organometallics 14 (1995) 4034–4036.
[8] D.I. Yoon, C.A. Berg-Brennan, H. Lu, J.T. Hupp, Synthesis and preliminary photophysical studies of intramolecular electron transfer in crown-linked donor- (chromophore-) acceptor complexes, Inorg. Chem. 31 (1992) 3192–3194.
[9] J.C. Calabrese, W. Tam, Organometallics for non-linear optics: metal-pyridine and bipyridine complexes, Chem. Phys. Lett. 133 (1987) 244–245.
[10] T.T. Ehler, N. Malmberg, K. Carron, B.P. Sullivan, L.J. Noe, Studies of organometallic self-assembled monolayers on Ag and Au using surface plasmon spectroscopy, J. Phys. Chem. B 101 (1997) 3174–3180.
[11] V.W.-W. Yam, V.C.-Y. Lau, K.-K. Cheung, Synthesis, photophysics and photochemistry of novel luminescent rhenium(I) photoswitchable materials, J. Chem. Soc. Chem. Commun. (1995) 259–261.
[12] B. Higgins, B.A. DeGraff, J.N. Demas, Luminescent transition metal complexes as sensors: structural effects on pH response, Inorg. Chem. 44 (2005) 6662–6669.
[13] U.N. Fagioli, F.S. García Einschlag, C.J. Cobos, G.T. Ruiz, M.R. Féliz, E. Wolcan, On the mechanism of Re(I)–carboxylate bond cleavage by perchloric acid: a kinetic and spectroscopic study, J. Phys. Chem. A 115 (2011) 10979–10987.
[14] S.C. Bottorff, A.L. Moore, A.R. Wemple, D.-K. Bučar, L.R. MacGillivray, P.D. Benny, PH-controlled coordination mode rearrangements of "Clickable" huisgen-based multidentate ligands with [MI(CO)3] + (M = Re, 99mTc), Inorg. Chem. 52 (2013) 2939–2950.
[15] A. Vlček, Ultrafast excited-state processes in Re(I) carbonyl-diimine complexes: from excitation to photochemistry, in: A.J. Lees (Ed.), Photophysics of Organometallics, Springer, Berlin/Heidelberg, 2010, pp. 73–114.
[16] A. Kumar, S.-S. Sun, A. Lees, Photophysics and photochemistry of organometallic rhenium diimine complexes, in: A.J. Lees (Ed.), Photophysics of Organometallics, Springer, Berlin/Heidelberg, 2010, pp. 37–71.
[17] M.-W. Louie, T.T.-H. Fong, K.K.-W. Lo, Luminescent Rhenium(I) polypyridine fluorous complexes as novel trifunctional biological probes, Inorg. Chem. 50 (2011) 9465–9471.
[18] K. Lo, Exploitation of luminescent organometallic Rhenium(I) and Iridium(III) complexes in biological studies, in: A.J. Lees (Ed.), Photophysics of Organometallics, Springer, Berlin/Heidelberg, 2010, pp. 73–114.
[19] K.K.-W. Lo, A.W.-T. Choi, W.H.-T. Law, Applications of luminescent inorganic and organometallic transition metal complexes as biomolecular and cellular probes, Dalton Trans. 41 (2012) 6021–6047.
[20] S.B. Jiménez-Pulido, M. Sieger, A. Knödler, O. Heilmann, M. Wanner, B. Schwederski, J. Fiedler, M.N. Moreno-Carretero, W. Kaim, Rhenium(I) coordinated lumazine and pterin derivatives: structure and spectroelectrochemistry of reversibly reducible (6-ATML)Re(CO)3Cl (6-ATML=6-acetyl-1,3,7-trimethyllumazine), Inorg. Chim. Acta 325 (2001) 65–72.
[21] C. Bessenbacher, C. Vogler, W. Kaim, Stabilization of biochemically interesting intermediates by metal coordination. 6. Charge transfer in complexes of 1,3-dimethyllumazine with low-valent metals, Inorg. Chem. 28 (1989) 4645–4648.
[22] O. Heilmann, F.M. Hornung, J. Fiedler, W. Kaim, Organometallic iridium(III) and rhenium(I) complexes with lumazine, alloxazine and pterin derivatives, J. Organomet. Chem. 589 (1999) 2–10.
[23] T. Kojima, T. Sakamoto, Y. Matsuda, K. Ohkubo, S. Fukuzumi, A Ruthenium pterin complex showing proton-coupled electron transfer: synthesis and characterization, Angew. Chem. Int. Ed. 42 (2003) 4951–4954.
[24] C. Lorente, A.H. Thomas, Photophysics and photochemistry of pterins in aqueous solution, Acc. Chem. Res. 39 (2006) 395–402.
[25] F. Ragone, G.T. Ruiz, O.E. Piro, G.A. Echeverría, F.M. Cabrerizo, G. Petroselli, R. Erra-Balsells, K. Hiraoka, F.S. García Einschlag, E. Wolcan, Water-soluble (Pterin)rhenium(I) complex: synthesis, structural characterization, and two reversible protonation–deprotonation behavior in aqueous solutions, Eur. J. Inorg. Chem. 2012 (2012) 4801–4810.
[26] Y. Gao, S. Sun, K. Han, Electronic structures and spectroscopic properties of rhenium (I) tricarbonyl photosensitizer: [Re(4,4′-(COOEt)2-2,2′-bpy)(CO)3py]PF6, Spectrochim. Acta A 71 (2009) 2016–2022.
[27] A. Vlcek Jr., S. Zális, Modeling of charge-transfer transitions and excited states in d6 transition metal complexes by DFT techniques, Coord. Chem. Rev. 251 (2007) 258–287.
[28] J. Dietrich, U. Thorenz, C. Förster, K. Heinze, Effects of sequence, connectivity, and counter ions in new amide-linked Ru(tpy)2–Re(bpy) chromophores on redox chemistry and photophysics, Inorg. Chem. 52 (2013) 1248–1264.
[29] D. Chartrand, C.A. Castro Ruiz, G.S. Hanan, Diimine triscarbonyl Re(I) of isomeric pyridyl-fulvene ligands: an electrochemical spectroscopic and computational investigation, Inorg. Chem. 51 (2012) 12738–12747.

[30] C. Zhao, C.S. Kambara, Y. Yang, A.L. Kaledin, D.G. Musaev, T. Lian, C.L. Hill, Synthesis, structures, and photochemistry of tricarbonyl metal polyoxoanion complexes, [X2W20O70{M(CO)3}2]12−(X = Sb, Bi and M = Re, Mn), Inorg. Chem. 52 (2013) 671–678.
[31] C.B. Anderson, A.B.S. Elliott, C.J. McAdam, K.C. Gordon, J.D. crowley, fac-Re(CO)3Cl complexes of [2-(4-R-1H-1,2,3-triazol-1-yl)methyl]pyridine inverse "Click" ligands: a systematic synthetic, spectroscopic, and computational study, Organometallics 32 (2013) 788–797.
[32] L. Yang, A.-M. Ren, J.-K. Feng, X.-D. Liu, Y.-G. Ma, H.-X. Zhang, Theoretical studies of ground and excited electronic states in a series of Rhenium(I) bipyridine complexes containing diarylethynyl-based structure, Inorg. Chem. 43 (2004) 5961–5972.
[33] L. Yang, A.-M. Ren, J.-K. Feng, X.-J. Liu, Y.-G. Ma, M. Zhang, X.-D. Liu, J.-C. Shen, H.-X. Zhang, Theoretical studies of ground and excited electronic states in a series of halide Rhenium(I) bipyridine complexes, J. Phys. Chem. A 108 (2004) 6797–6808.
[34] S. Záliš, C.J. Milne, A. El Nahhas, A.M. Blanco-Rodríguez, R.M. van der Veen, A. Vlček, Re and Br X-ray absorption near-edge structure study of the ground and excited states of [ReBr(CO)3(bpy)] interpreted by DFT and TD-DFT calculations, Inorg. Chem. 52 (2013) 5775–5785.
[35] J. Bossert, C. Daniel, Trans–cis photoisomerization of the styrylpyridine ligand in [Re(CO)3(2,2′-bipyridine)(t-4-styrylpyridine)]+: role of the metal-to-ligand charge-transfer excited states, Chem. Eur. J. 12 (2006) 4835–4843.
[36] P. Hohenberg, W. Kohn, Inhomogeneous electron gas, Phys. Rev. 136 (1964) B864–B871.
[37] W. Kohn, L.J. Sham, Self-consistent equations including exchange and correlation effects, Phys. Rev. 140 (1965) A1133–A1138.
[38] R.G. Parr, W. Yang, Density Functional Theory of Atoms and Molecules, Oxford University Press, 1989.
[39] M.J. Frisch, G.W. Trucks, H.B. Schlegel, G.E. Scuseria, M.A. Robb, J.R. Cheeseman, G. Scalmani, V. Barone, B. Mennucci, G.A. Petersson, H. Nakatsuji, M. Caricato, X. Li, H.P. Hratchian, A.F. Izmaylov, J. Bloino, G. Zheng, J.L. Sonnenberg, M. Hada, M. Ehara, K. Toyota, R. Fukuda, J. Hasegawa, M. Ishida, T. Nakajima, Y. Honda, O. Kitao, H. Nakai, T. Vreven, J.J.A. Montgomery, J.E. Peralta, F. Ogliaro, M. Bearpark, J.J. Heyd, E. Brothers, K.N. Kudin, V.N. Staroverov, T. Keith, R. Kobayashi, J. Normand, K. Raghavachari, A. Rendell, J.C. Burant, S.S. Iyengar, J. Tomasi, M. Cossi, N. Rega, J.M. Millam, M. Klene, J.E. Knox, J.B. Cross, V. Bakken, C. Adamo, J. Jaramillo, R. Gomperts, R.E. Stratmann, O. Yazyev, A.J. Austin, R. Cammi, C. Pomelli, J.W. Ochterski, R.L. Martin, K. Morokuma, V.G. Zakrzewski, G.A. Voth, P. Salvador, J.J. Dannenberg, S. Dapprich, A.D. Daniels, O. Farkas, J.B. Foresman, J.V. Ortiz, J. Cioslowski, D.J. Fox, Gaussian 09, Revision A1, Gaussian, Inc., Wallingford, CT, 2009.
[40] A.D. Becke, Density-functional thermochemistry. III. The role of exact exchange, J. Chem. Phys. 98 (1993) 5648–5652.
[41] C. Lee, W. Yang, R.G. Parr, Development of the Colle-Salvetti correlation-energy formula into a functional of the electron density, Phys. Rev. B 37 (1988) 785–789.
[42] T.H. Dunning Jr., P.J. Hay, in: H.F. Schaefer III (Ed.), Methods of Electronic Structure Theory, Plenum Press, 1977.
[43] P.J. Hay, W.R. Wadt, Ab initio effective core potentials for molecular calculations. Potentials for the transition metal atoms Sc to Hg, J. Chem. Phys. 82 (1985) 270–283.
[44] P.J. Hay, W.R. Wadt, Ab initio effective core potentials for molecular calculations. Potentials for K to Au including the outermost core orbitals, J. Chem. Phys. 82 (1985) 299–310.
[45] W.R. Wadt, P.J. Hay, Ab initio effective core potentials for molecular calculations. Potentials for main group elements Na to Bi, J. Chem. Phys. 82 (1985) 284–298.
[46] R. Bauernschmitt, R. Ahlrichs, Treatment of electronic excitations within the adiabatic approximation of time dependent density functional theory, Chem. Phys. Lett. 256 (1996) 454–464.
[47] M.E. Casida, C. Jamorski, K.C. Casida, D.R. Salahub, Molecular excitation energies to high-lying bound states from time-dependent density-functional response theory: Characterization and correction of the time-dependent local density approximation ionization threshold, J. Chem. Phys. 108 (1998) 4439–4449.
[48] R.E. Stratmann, G.E. Scuseria, M.J. Frisch, An efficient implementation of time-dependent density-functional theory for the calculation of excitation energies of large molecules, J. Chem. Phys. 109 (1998) 8218–8224.
[49] D. Feller, The role of databases in support of computational chemistry calculations, J. Comput. Chem. 17 (1996) 1571–1586.
[50] K.L. Schuchardt, B.T. Didier, T. Elsethagen, L. Sun, V. Gurumoorthi, J. Chase, J. Li, T.L. Windus, Basis set exchange: a community database for computational sciences, J. Chem. Inf. Model. 47 (2007) 1045–1052.
[51] V. Barone, M. Cossi, Quantum calculation of molecular energies and energy gradients in solution by a conductor solvent model, J. Phys. Chem. A 102 (1998) 1995–2001.
[52] M. Cossi, V. Barone, Time-dependent density functional theory for molecules in liquid solutions, J. Chem. Phys. 115 (2001) 4708–4717.
[53] B. Mennucci, J. Tomasi, Continuum solvation models: a new approach to the problem of solute's charge distribution and cavity boundaries, J. Chem. Phys. 106 (1997) 5151–5158.
[54] E.D. Glendening, A.E. Reed, J.E. Carpenter, F. Weinhold, NBO Version 3.1.
[55] S.I. Gorelsky, A.B.P. Lever, Electronic structure and spectra of ruthenium diimine complexes by density functional theory and INDO/S. Comparison of the two methods, J. Organomet. Chem. 635 (2001) 187–196.
[56] S.I. Gorelsky, AOMix Program, Revision 6.81, <http://www.sg-chem.net/>.
[57] N. O'Boyle, GaussSum 2.2.5 Program Documentation <http://gausssum.sourceforge.net/GaussSum_UVVis_Convolution.pdf>.
[58] F. Weinhold, C.R. Landis, Natural bond orbitals and extensions of localized bonding concepts, Chem. Educ. Res. Pract. 2 (2001) 91–104.
[59] H.H. Martinez Saavedra, C.A. Franca, G. Petroselli, R. Erra-Balsells, G.T. Ruiz, E. Wolcan, A new zwitterionic, water soluble, Re(I) complex: synthesis, spectroscopic and computational characterization, J. Organomet. Chem. 745–746 (2013) 470–478.
[60] S.I. Gorelsky, A.B.P. Lever, The electronic structure and spectra of [Ru(NH3)4(LL)]2+ (LL = bpy, bpz, bqdi) studied by density functional theory and INDO/S. Charge transfer character of electronic transitions and their solvatochromism, Can. J. Anal. Sci. Spectrosc. 48 (2003) 93–105.